



MODELING OF A COMMERCIAL PIEZOELECTRIC ENERGY HARVESTING DEVICE THROUGH EXPERIMENTAL IDENTIFICATION

Marcel Araujo Clementino

Carlos De Marqui Junior

Department of Aeronautical Engineering, Engineering School of Sao Carlos - University of Sao Paulo, Av. Trabalhador Sancarlene 400, 13566-590, São Carlos, SP, Brazil

marcelclementino@usp.br

demarqui@sc.usp.br

Samuel da Silva

UNESP - Univ Estadual Paulista, Faculdade de Engenharia de Ilha Solteira, Departamento de Engenharia Mecânica, Campus de Ilha Solteira, Av. Brasil, n° 56, 15385-000, Ilha Solteira, SP.

samuel@dem.feis.unesp.br

Abstract. *The energy harvesting literature shows that several devices have been developed covering many applications either in academic or commercial purpose. However, these devices may not be suitable for practical situations, or somehow may limit its application due to the lack of important data or characteristics. Thus, an experimental analysis may be useful in order to verify the behavior of these devices and estimate some unknown parameters. In this sense, this paper presents experimental tests carried out with a commercial energy harvesting device, given by a cantilever piezoelectric beam and a circuit for extracting/storing energy. A spring-mass-damper single degree of freedom (SDOF) model of the piezoelectric generator is experimentally identified and the results verified against experimental results. The modeling procedure uses the modal parameters of the system (natural frequency and damping rate), which are also experimentally estimated, and allow considering different topologies for the harvesting circuit, including the more complex ones. Furthermore, the behavior of the commercial circuit is compared to a resistive circuit and a full-wave diode bridge. The model proves to be capable for simulating the conditions of a typical vibration based energy harvesting environment and the results confirmed the necessity of controlling the energy harvested by the piezoelectric generator.*

Keywords: *energy harvesting, experimental analysis, circuit comparison, system identification*

1. INTRODUCTION

Over the last ten years, much attention has been given to the use of piezoelectric materials in the energy harvesting scenario, mainly concerning the transformation of vibration energy into electrical energy (Sodano *et al.*, 2004a; Anton and Sodano, 2007; Cook-Chennault *et al.*, 2008a). Most of the researchers focus their efforts on the concept of self-powered wireless devices, usually applied in structural health monitoring (SHM) systems, where there is a necessity to avoid the human intervention over the devices. Therefore, while some authors are concerned with the modeling approaches of the harvester, either by modeling complex electromechanical structures with simplified electrical circuits (Sodano *et al.*, 2004a; duToit *et al.*, 2005; Erturk and Inman, 2008a; Miller *et al.*, 2011; Masana and Daqaq, 2012), or complex harvesting circuit with simplified structure models (Guyomar *et al.*, 2005; Lefeuvre *et al.*, 2007; Lallart *et al.*, 2008, 2011; Liang and Liao, 2012), or even considering the interaction between complex structures and circuits (Yang and Tang, 2009; Elvin and Elvin, 2009; Chen and Pan, 2011; Wang *et al.*, 2012), others are interested in the behavior of these harvesters in certain applications.

Indeed, the evolution of these researches in the energy harvesting field and the reduction of the required power level of novel electronic devices has brought the piezoelectric harvesters more close to everyday activities. One of the very well known applications is related with the use of energy harvesting devices in shoes, which enables the conversion of the energy spent by the heel strike during a person's walk. Kymissis *et al.* (1998) were among the pioneers that studied this type of application. Recently, Howells (2008) presented a device developed by the U.S army that follows the same purpose. The device is given by 4 bimorph piezoceramic (PZTs) stacks and is able to produce 90 mW in average, power that is enough to supply a basic cellphone on stand-by condition (when it consumes around 42 mW). Still trying to use the human body movement to generate energy, Pozzi *et al.* (2012) developed a piezoelectric device to harvest energy from the movement of the knee joint. Their device was tested in a machine that simulates this type of motion, considering several footstep patterns of a person that carries a backpack with different weights and 2 mW was delivered in average.

Kalyanaraman and Babu (2010) proposed the use of piezoelectric patches under cellphone and laptop keys, in order to harvest energy as the user press them. Along the harvesting procedure, the energy was rectified and stored in a capacitor to charge a secondary battery that assists the main battery in an emergency situation. A PVDF membrane disposed in the stack form was installed under the keys in order to harvest the energy, reaching 1.2 W.

Therefore, by conducting a brief research over the energy harvesting field, it is possible to observe that several devices have already been developed, either with academic or commercial purpose. However, this range of devices may not cover certain applications, or somehow may limit it due to the lack of important data or characteristics. In these cases, it may be interesting to analyze their behavior using experimental tests that may also allow to estimate some unknown parameters.

In this paper, a SDOF model of a commercial piezoelectric harvester is experimentally identified by estimating the harvester modal parameters (natural frequency and damping ratio). Different topologies can be considered for the harvesting circuit. Therefore, three different circuits are considered: a resistive circuit, a full-wave diode bridge and a commercial circuit. Simulations are carried out for the three cases regarding different excitation frequencies and resistive loads. The numerical predictions are verified against experimental results.

2. DESCRIPTION OF THE ENERGY HARVESTING SYSTEM

The system described in this section, called Piezoelectric Energy Harvesting Kit, is manufactured by Piezo Systems, Inc.. The kit includes a bimorph piezoelectric beam (without a metallic substructure) and a extraction/storage circuit, as shown in Fig. 1. The piezoelectric elements are connected in parallel to increase the electrical current, since the harvester aims to supply energy to a storage device, like a capacitor.

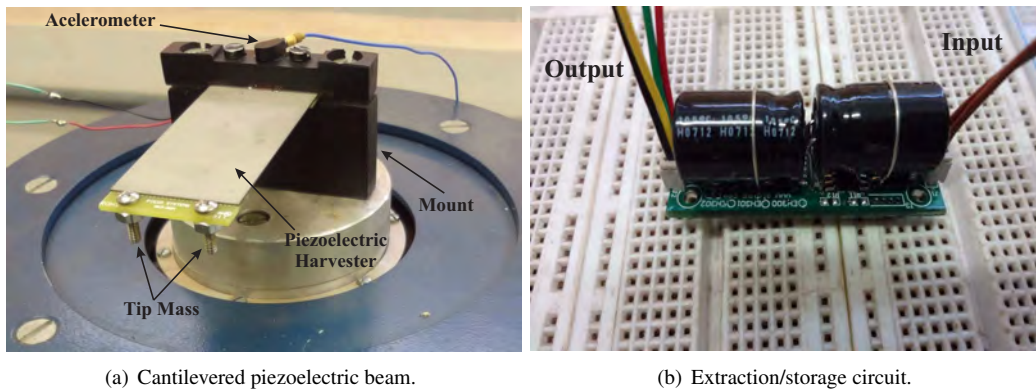


Figure 1. Commercial energy harvesting system.

Figure 1(a) shows the cantilevered piezoelectric beam, which was subjected to harmonic motion of the cantilevered end during the experimental tests. The base acceleration of the harvester is measured by a low mass accelerometer (352C22 from PCB). In addition, a tip mass is attached to the free end of the harvester to reduce its natural frequency and enhance its flexibility, once the vibration sources available for energy harvesting have relatively low frequencies.

The extraction/storage circuit, shown in Fig. 1(b), includes in its topology a rectifier circuit, to perform the AC/DC transformation, and a capacitors to store the energy harvested. Therefore, when the electromechanical system vibrates, the piezoelectric beam converts vibration energy into electrical energy and, hence, the alternate voltage produced is transformed into direct voltage by an electronic circuit, as shows the schematics in Fig. 2(a). Thus, the energy is stored in the capacitors to be used according to the desired application and load requirements.

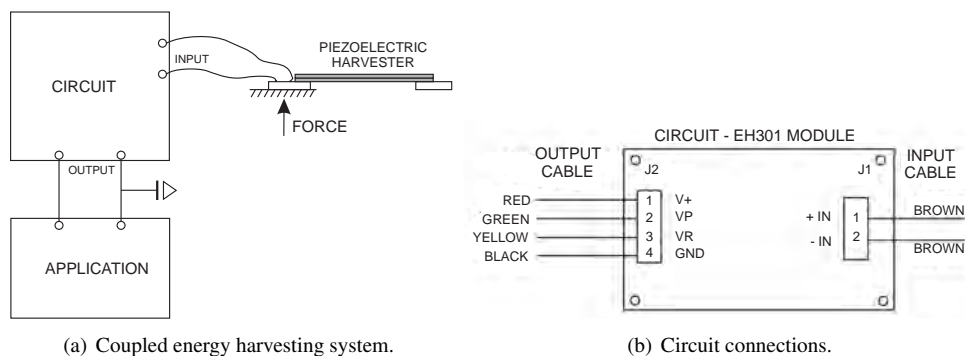


Figure 2. Schematics of the energy harvesting system(Advanced Linear Devices, 2012).

Figure 2(b) shows an scheme of the extraction circuit, which includes two input terminals, positive and negative, and four output terminals: **V+**, **VP**, **VR** and **GND** (reference); where **VR** and **V+** are used for voltage monitoring and **VP** is used to supply energy to the load.

Initially, there is no voltage across the capacitor, i.e. $V+$ is zero. When the harvester is excited the capacitor is charged until $V+$ reaches a VH value, that enables the circuit output. Consequently, the stored energy supplies the load and, therefore, three situations may occur:

- The energy supplied by the piezoelectric harvester (voltage source) is enough to keep the capacitors loaded and also supply the load. Thus, the voltage across the load $V+$, remains constant;
- The energy from the source is greater than the load demands. Thus, the voltage across the capacitors increases until a cut-off value is reached, VC , when the circuit stops the energy storage and the voltage $V+$ starts decreasing.
- The source can not maintain the load and $V+$ decreases as soon as the stored energy is released to the load.

Either way, case the supplied voltage is not enough to keep the capacitor charged, the voltage across the capacitor decreases until it attain a VL value. From this point, the controlled circuit also stops the voltage supply from the capacitors to the load, disconnecting the load from the circuit. Therefore, the charge cycle of the capacitors starts over again. Table 1 presents the main characteristics of the beam and the circuit. Detailed information can be found in the manufacturer catalog (Advanced Linear Devices, 2012).

Table 1. Main parameters of the commercial energy harvesting system (Advanced Linear Devices, 2012).

Circuit		Piezoelectric beam	
Model	EH301A	PZT Model	5A4E
Lower voltage bound (VL)	3.10 V	Length (L_p)	76.20 mm
Upper voltage bound (VH)	5.20 V	Width (w)	31.80 mm
Cut-off voltage (VC)	6.80 V	Thickness (t_p)	0.508 mm
Useful output energy	55.00 mJ	Capacitance (C_p)	232.00 nF
Maximum output current	1.00 A	-	-

The harvester is excited with an electromagnetic shaker. The sine signal was generated with a USB-6251 Data Acquisition board, controlled by LabView software, and was amplified by a power amplifier. The base acceleration of the harvester is measured by a low mass accelerometer (352C22 from PCB and sensor signal conditioner 480E09 from PCB). Figure 3 shows the experimental setup and the equipment used in the tests.

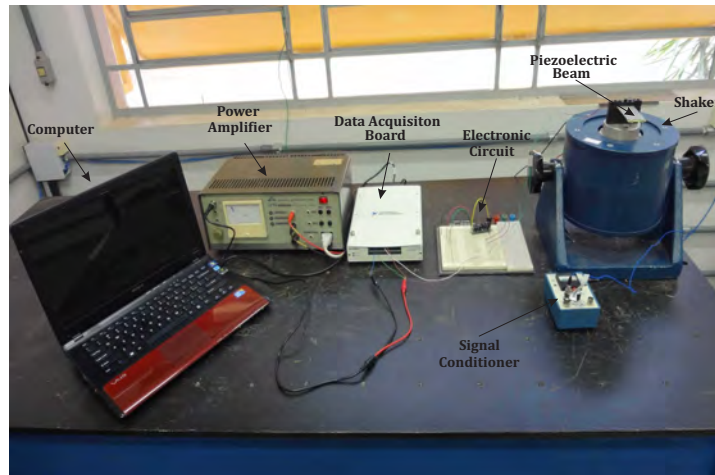
Three different cases are considered in the experiments: 1 - the harvester is in open circuit condition, 2 - the harvester is connected to a load resistance and 3 - the harvester is connected to an extraction/storage circuit. In all three cases, the voltage and acceleration values were measured using the USB-6251 DAQ board and the data acquisition and processing were performed using Matlab.

3. SDOF MODEL OF THE PIEZOELECTRIC HARVESTER

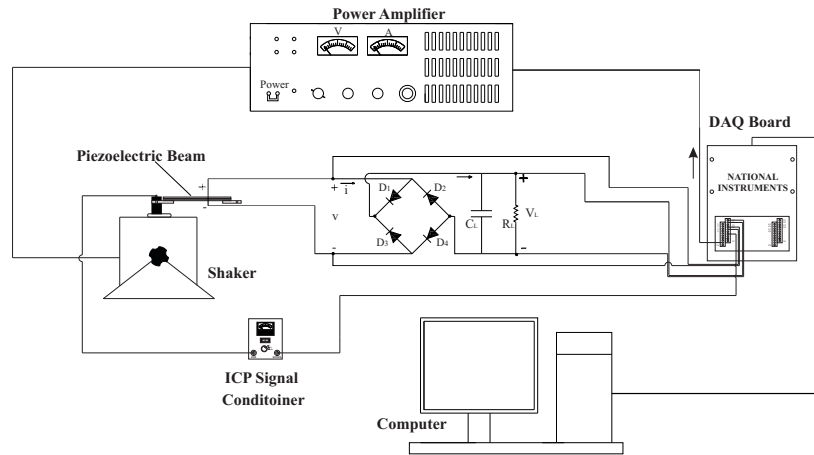
A single degree of freedom (SDOF) model is proposed in order to describe the electromechanical behavior of the piezoelectric energy harvesting device. One of the major research challenges in the field of piezoelectric energy harvesting includes the ability of accurately modeling and designing these coupled electromechanical systems. Many authors (Sodano *et al.*, 2004b; duToit *et al.*, 2005; Liao and Sodano, 2008) have included only a simple load resistance in the electrical domain of the problem. However, most circuits that are attached to the piezoelectric harvester are more complex than a single resistor and might include nonlinear elements. The modeling of these circuits would require electronic circuit simulators. To address this issue, Elvin and Elvin (2008) presented an equivalent circuit model in order to represent the electromechanical system and circuit in an electronic circuit simulator (SPICE). In this paper a different approach is presented. The Matlab/Simulink is used to represent the electromechanical system and electrical circuits. This way, different electrical circuits, ranging from a simple load resistance to more realistic circuits, can be considered (Clementino *et al.*, 2013). Following the procedure presented by Clementino *et al.* (2013) the electromechanical model as well as the different electrical circuits considered in this work are a resistive circuit, a full-wave diode bridge and a commercial circuit.

Due to the lack of information about the commercial harvesting system, such as type of materials used in the harvester and circuit components, for example, it is more convenient to use a lumped parameters modeling approach because the harvester model can be experimentally estimated and the analyzed system is only excited by the first natural frequency. Moreover, the SDOF approach for piezoelectric energy harvesters will not be covered in details here and only the equation of motion will be provided, since it is already a consolidated and very well discussed subject in the literature. Further information about this approach can be found in (Erturk and Inman, 2008b, 2009; Roundy and Wright, 2004; duToit *et al.*, 2005; Chen *et al.*, 2006).

M. A. Clementino, C. De Marqui Jr. and S. da Silva
SDOF modeling of a commercial piezoelectric energy harvesting device through experimental identification



(a) Equipment view.



(b) Schematics of the experimental setup.

Figure 3. Experimental setup used during the tests.

The harvester equation of motion is described in terms of the natural frequency (ω_n) and damping ratio (ξ), for the mechanical domain, and piezoelectric capacitance (C_p), for the electrical domain, where both domains are coupled by the electromechanical coupling factor (Θ). This equation can be written as follows (duToit *et al.*, 2005)¹:

$$\ddot{r} + 2\xi\omega_n\dot{r} + \omega_n^2 r - \frac{\Theta}{M}v = \mu_1 \frac{|a_{base}|}{M} \sin(\omega t) \quad (1)$$

$$\Theta\dot{r} + C_p\dot{v} + \dot{q} = 0 \quad (2)$$

where r , \dot{r} and \ddot{r} are, respectively, the transverse displacement, velocity and acceleration of the harvester; v is the voltage output, \dot{q} is the current that flows into the circuit and feeds back the piezoelectric elements, a_{base} is the base acceleration, M is the harvester mass, ω is the base vibration frequency and μ_1 is the correction factor for a uniform beam with a tip mass (M_c) subjected to transverse vibrations, given by (Erturk and Inman, 2008c):

$$\mu_1 = \frac{(M_c/M)^2 + 0,603(M_c/M) + 0,08955}{(M_c/M)^2 + 0,4637(M_c/M) + 0,05718} \quad (3)$$

According to Erturk and Inman (2008c), this correction factor considers the contribution of the distributed mass on the excitation amplitude, which must be considered in case the tip mass is not relatively large. In this paper, the tip mass to the beam mass ratio $M_t/M = 0,22$ is low, thus a correction factor $\mu_1 = 1,3$ must be used. In addition, it was necessary to perform a modal parameter identification, i.e. natural frequency (ω_n) and damping ratio (ξ), to obtain the harvester model.

¹This reference presents the equation of motion for a system under strain along the 3 axis and, thus, considers the piezoelectric constant d_{33} when defining the electromechanical coupling factor. On the other hand, in the present paper the d_{31} constant is considered since the strain occurs along 1 axis.

Therefore, a Frequency Response Function (FRF) of the electromechanical system was calculated using the shaker supply voltage as input signal and the voltage produced by the piezoelectric beam as output signal. The FRF was estimated considering the PZTs in open circuit condition, while the input was a pseudo-random signal (Gaussian noise) filtered by a 4th order Butterworth low-pass filter, with $f_c = 100$ Hz as cut-off frequency. This frequency was chosen to limit the frequency bandwidth that excited the beam to a range that included only its first natural frequency. Figure 4 shows the input and output signals used in the estimation.

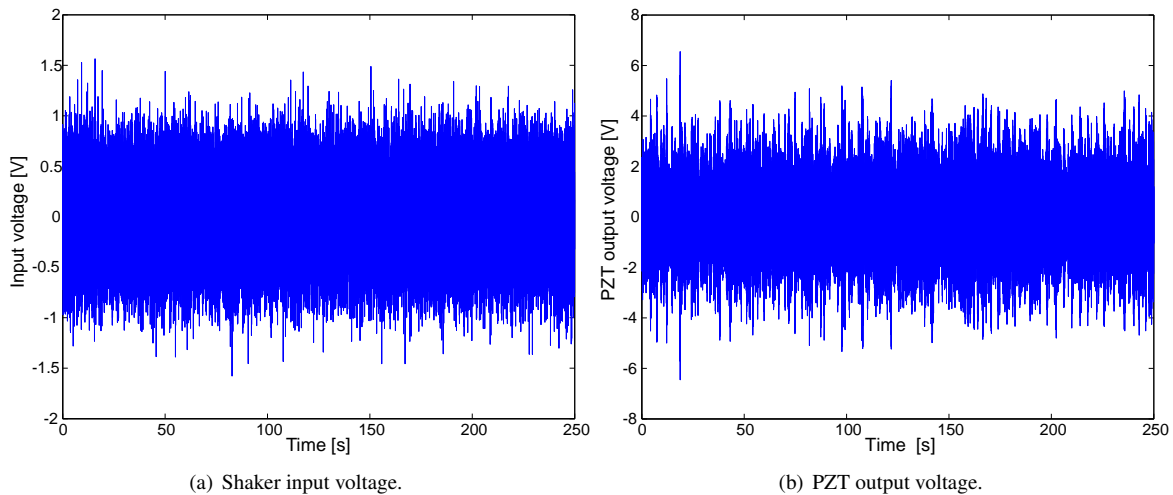


Figure 4. Input and output signals used to estimate the FRF of the electromechanical system.

The data acquisition was carried out using a sampling rate of 400 sample/s and a total of 100×10^3 samples that allowed to calculate the FRF using the H_1 estimator, with 50% overlap, Hanning window and 100 averages. Both, the natural frequency and the damping ratio, could be determined from the FRF. The first was obtained from the FRF amplitude peak and the latter using the Quadrature Peak Picking method, which consists on taking two frequencies, ω_1 e ω_2 , around the resonance peak (known as half power point) and estimate the damping ratio by the following relation (Inman, 2001):

$$\xi = \frac{\omega_2 - \omega_1}{2\omega_n}. \quad (4)$$

Figure 5 shows the estimated FRF and the characterization of the half power point. The values obtained from the FRF were: $\omega_1 = 277.720$ rad/s, $\omega_2 = 287.393$ rad/s, $\omega_n = 281.487$ rad/s (open circuit) and $\xi = 0.017$. After estimating the system modal parameters, it remains to determine the electromechanical coupling factor (Θ), as it is not informed by the manufacturer. In this case, a optimization procedure was performed in order to estimate the coupling factor. The optimization variable was $x = \Theta$ and the objective function ($f(x)$) to be minimized was the difference between the RMS voltage produced by the PZTs (calculated using the steady state voltage signal) predicted by the model (v_{pred}) and the voltage experimentally measured (v_{exp}). Thus, the optimization problem could be described as follow:

$$\text{Minimize } f(x) = \sqrt{(v_{pred}^{rms} - v_{exp}^{rms})^2}$$

where the optimization variable is

$$x = \Theta \quad (5)$$

subjected to the following constraint:

$$j(x) : \Theta \leq \Theta^{min}. \quad (6)$$

To implement this procedure it was used the Sequential Quadratic Programming as optimization method along with the *fmincon* function, to obtain an initial estimative, and the *GlobalSearch* function, to search for a global minimum of the problem. The *GlobalSearch* function tests several initial conditions and finds a global minimum inside the set of local minima, where each minimum corresponds to a different initial condition². Hence, by limiting the optimization variable to $\Theta \leq 10^{-7}$ and using $x_o = 1,4191 \times 10^{-4}$ as initial condition, it was possible to achieve $\Theta = 1,3508 \times 10^{-5}$, as it is shown in Fig. 6. A variation less than 1×10^{-10} in the optimization parameter was set as the stop criterion, which led to $f = 3,1746 \times 10^{-5}$.

²Additional information can be found in Matlab user guide under *Global Optimization Toolbox* section.

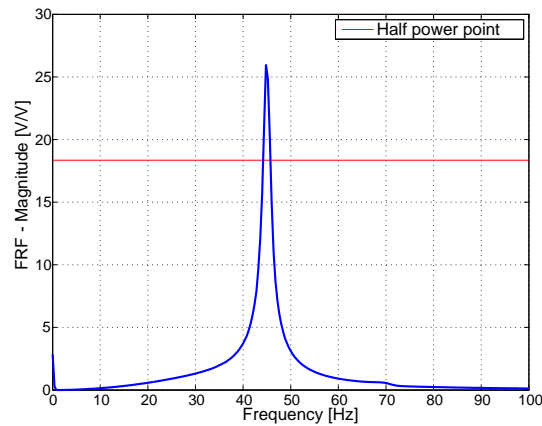


Figure 5. Estimative of the voltage FRF for PZTs in open circuit condition.

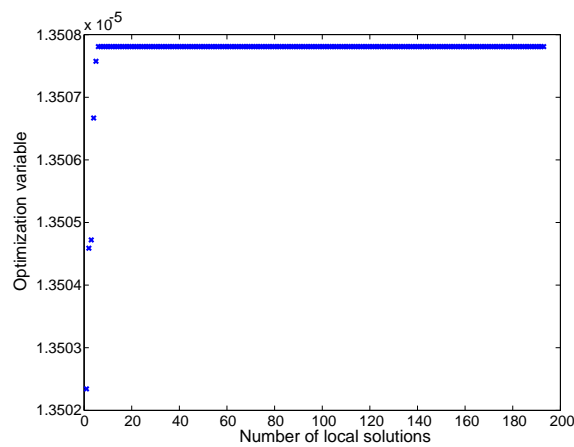


Figure 6. Evolution of the optimization variable along the problem solution.

On the other hand, since the maximum power is extracted only when the impedance of the piezoelectric harvester and the electronic circuit are matched (situation known as "impedance matching"), the condition which this situation occur must be determined. In this sense, the curve that represents the behavior of the power harvested against the resistive load (considering the open circuit natural frequency, $f = 44.8$ Hz, as excitation frequency) was obtained and a optimum resistance $R_{opt} = 33$ k Ω was verified, as shows Fig. 7. This curve was estimated using values of voltage measured across the load for different resistive loads. The power transferred to the load was calculated considering the RMS value of the alternate steady state voltage signal.

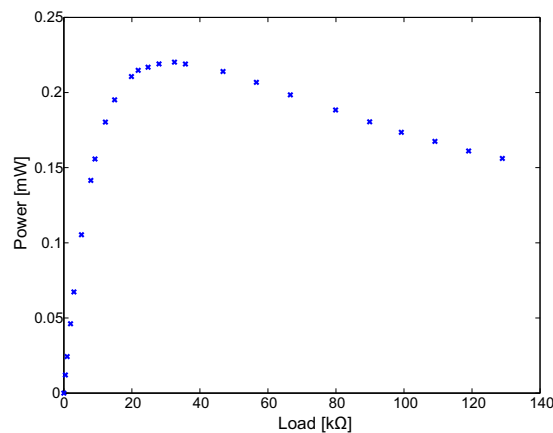


Figure 7. Influence of the resistive load on the power harvested considering the $f = 44$ Hz as excitation force.

Likewise defining the electromechanical model of the energy harvester, it is also of interest to model the whole energy harvesting system, and thus, consider the connection between the structure and the circuit. The proposed modeling procedure accounts for this effect using Simulink as an effective software package to simulate the mechanical and

electrical/electronic components of the circuit. Therefore, the harvester model can be described using a state-space representation and this allows it to be connected to an extraction/storage circuit. For a SDOF electromechanical model, the state-space realization can be written as:

$$\dot{\mathbf{x}} = \mathbf{Ax} + \mathbf{Bu} \tag{7}$$

$$\mathbf{y} = \mathbf{Cx} + \mathbf{Du} \tag{8}$$

where

$$\begin{aligned} \mathbf{A} &= \begin{bmatrix} 0 & 1 & 0 \\ -\omega_n^2 & -2\xi\omega_n & \frac{\Theta}{m} \\ 0 & -\frac{\Theta}{C_p} & 0 \end{bmatrix} \\ \mathbf{B} &= \begin{bmatrix} 0 & 0 \\ 1.3\frac{a_{base}\epsilon}{m} & 0 \\ 0 & \frac{1}{C_p} \end{bmatrix} \\ \mathbf{C} &= \begin{bmatrix} 0 & 0 & 1 \end{bmatrix} \\ \mathbf{D} &= \begin{bmatrix} 0 & 0 \end{bmatrix} \end{aligned} \tag{9}$$

The state vector is $\mathbf{x} = \{\mathbf{r}(t) \quad \dot{\mathbf{r}}(t) \quad v(t)\}^T$, \mathbf{A} is the dynamic matrix, \mathbf{B} the input matrix, \mathbf{C} the output matrix and \mathbf{D} is the direct transmission matrix. The output matrix \mathbf{C} provides the output $y = v(t)^T$ and the input vectors are defined by $u_1 = \sin(\omega t)$ and $u_2 = \dot{q}(t)$, where u_1 is multiplied by a_{base} to produce the external force applied in the clamped base of the beam. The electrical current $\dot{q}(t)$ results from the rectifier and load circuits attached to the output voltage $v(t)$, and is then fed back into the state-space model. This connection is shown in Fig. 8, where a full-wave bridge rectifier is connected to the harvester. However, this modeling approach does not restrict the circuit topology to have only passive elements, allowing to use switching elements (e.g., bipolar junction transistors) as it is shown in the remainder of this section.

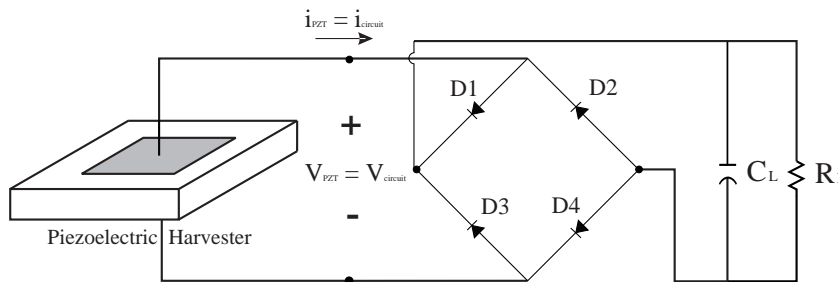


Figure 8. Schematics of the piezoelectric harvester coupled to a rectifier circuit.

4. RESULTS

The numerical tests were performed considering three topologies for the harvesting circuit: a resistive circuit, full wave bridge rectifier and the commercial harvesting circuit. The simulations and tests were carried out according to the configuration set given in Tab. 2.

Table 2. Cases analyzed in the experimental tests.

Tests	Parameters	Circuit Type		
		Resistive	Full wave bridge rectifier	EH301A (commercial)
1	$f = 44.80 \text{ Hz}, R_L = 33.00 \text{ k}\Omega$	X	X	X
2	$f = 21.50 \text{ Hz}, R_L = 33.00 \text{ k}\Omega$			X
3	$f = 44.80 \text{ Hz}, R_L = 80.00 \text{ k}\Omega$		X	X

4.1 Case A - Resistive circuit

For the resistive case, represented in Fig. 9, only the test 1 of Tab. 2 was performed ($f = 44.8 \text{ Hz}$ and $R = 33 \text{ k}\Omega$). The base acceleration was set to $a_{rms} = 0.073 \text{ g}$ (Fig. 10(a)) for this and the other cases that considered test 1.

As it was expected, the results shows that without the rectifier circuit the voltage across the load (Fig. 10(b)) has alternate characteristic. Therefore, the output signal can not be used properly in a practical application, since ordinary low powered devices requires a DC power supply signal. However, the main point observed from Fig. 10(b) is that the model successfully predicts the experimental results.

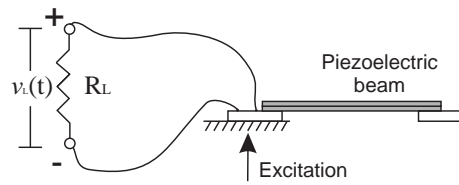


Figure 9. Schematics of the piezoelectric harvester connected to the resistive circuit.

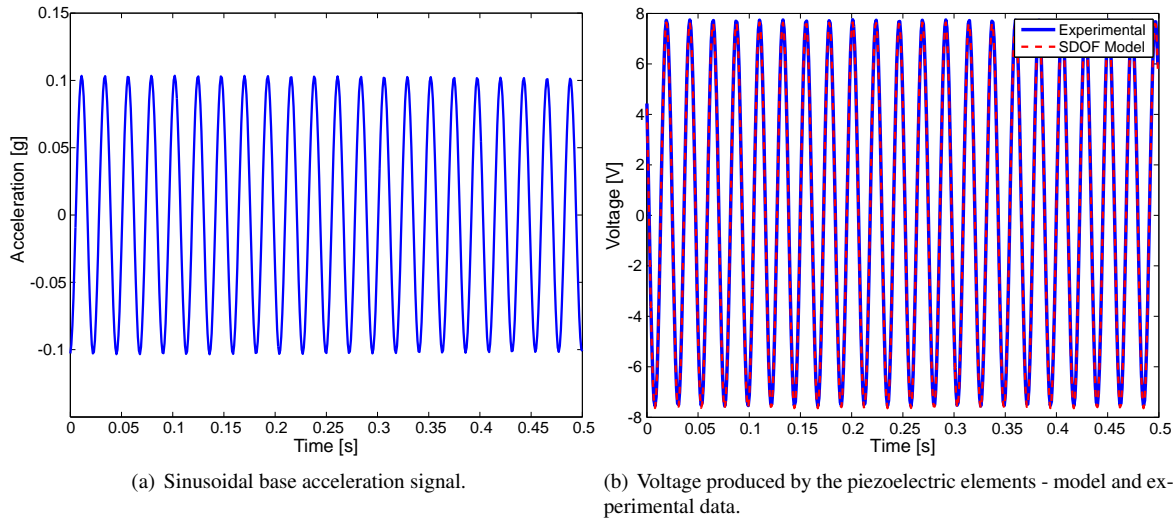


Figure 10. Input and output signals for the resistive case.

4.2 Case B - Full wave bridge rectifier

In this case, a full wave bridge rectifier with a capacitive filter is considered, as it is shown in Fig. 11. Since passive rectifiers were already extensively discussed in the literature, a detailed description of it is not given here.

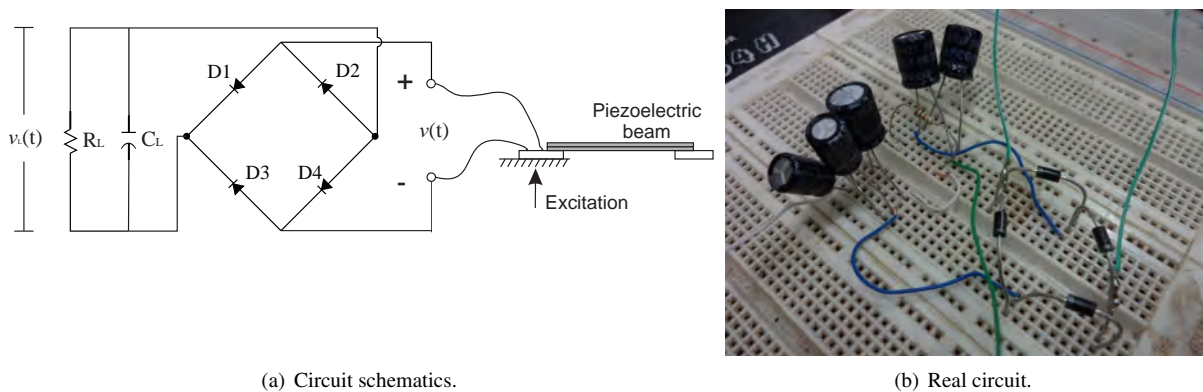


Figure 11. Full wave bridge rectifier with a capacitive filter.

The circuit topology was given by four 1N5817 Schottky diodes, a load resistance of $33 \text{ k}\Omega$ (R_L), and a capacitive filter made by five parallel capacitors ($C_L = 2 \times 220 \mu\text{F} + 3 \times 470 \mu\text{F} = 1850 \mu\text{F}$). Tests 1 and 4 were performed for this case and the base acceleration was the same as case 1, once it depends on the excitation frequency ($a = A\omega^2$), which was not changed.

One can note in Fig. 12 that the model successfully predicts the experimental results, although noise is verified in the experimental signal. This can be attributed to the non-ideal connection of the measurement probes. Nevertheless, this circuit does not have a control of the output energy and is proper to be used in applications that continuously requires a power supply. Next section shows the commercial circuit and a similar one that executes the same task, both able to

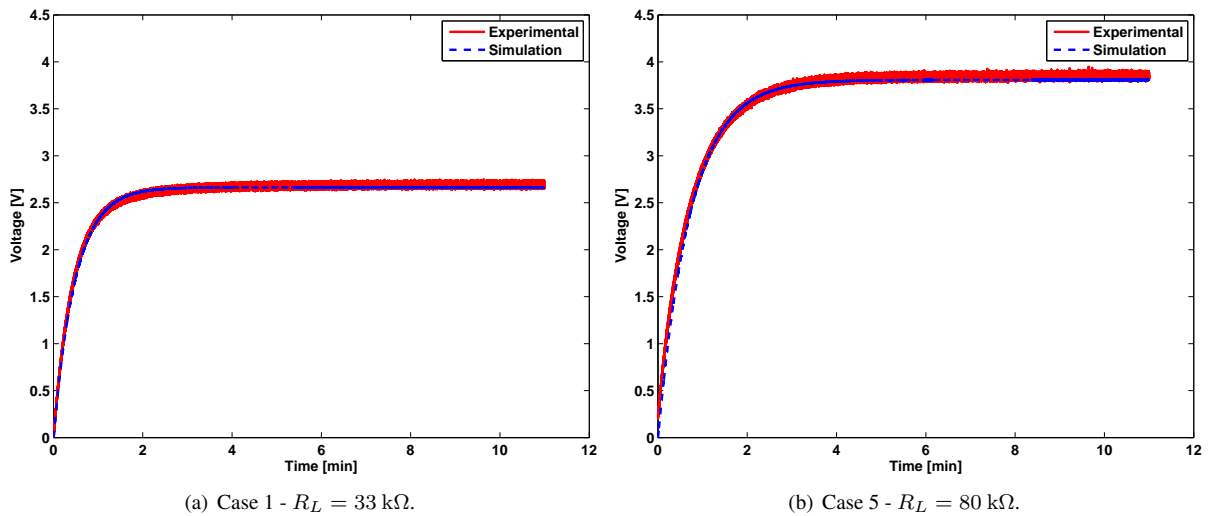


Figure 12. Voltage across the load for different loads in the full wave bridge rectifier circuit.

manage the energy harvested. This illustrates the ability of the proposed modeling approach while performing simulations with more complex harvesting circuits.

4.3 Case C - Commercial circuit

In this case, all tests of Tab. 2 were performed and, by having the voltage across the load monitored, it was also possible to evaluate the charge/discharge time for each test. However, since this is a commercial circuit most information about the circuit topology, as well as the parameters used, are not available for the users and customers. In other words, there is no way of knowing the topology of the circuit and, therefore, there is no means to model this circuit ensuring that exactly the same components are used. Thus, in order to compare the numerical and experimental results, it was proposed a circuit (Fig. 13) that includes only passive elements and executes the same task as the commercial circuit, instead of seeking the exact one.

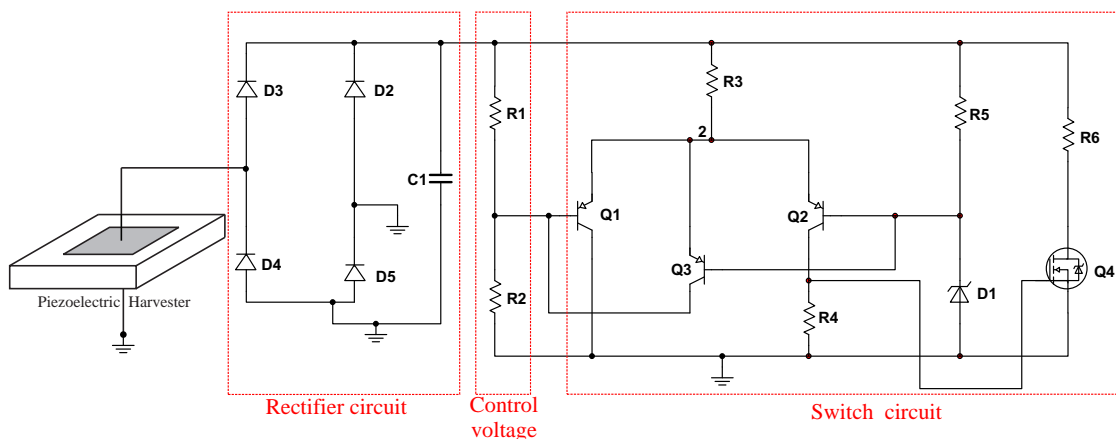


Figure 13. Schematics of the proposed harvesting circuit that simulates the commercial EH301A.

The circuit in Fig. 13 can basically be divided in three parts, the rectifier, the voltage control circuit and the switching circuit. The first part is responsible for the AC/DC conversion and the latter performs the connection between the storage capacitor and the external load, i.e. the resistance. The full wave rectifier has the same parameters as presented in case B, except by the storage capacitor, which has a capacitance $C_L = 6600 \mu\text{F}$.

Considering the switching circuit, it can be seen that its main components are three Bipolar Junction Transistors (BJTs), one Zener diode and a N-Channel MOSFET. The voltage control circuit (given by a voltage divider, R_1 and R_2) is used to set the voltage across the base of the Q_1 transistor, which has its emitter connected to the Q_2 transistor (Q_1 and Q_2 are the same). The Zener diode is connected to the base of Q_2 and its Zener voltage (V_z) is used as set-point to execute the switching task. So, as the voltage across the base of Q_1 reaches V_z , both Q_1 and Q_2 are in the saturation region, conducting current to base of the N-Channel MOSFET (Q_4). Q_4 also starts conducting and, therefore, connects

the storage capacitor and the load (R_6). Figure 14 shows the results achieved with the three tests.

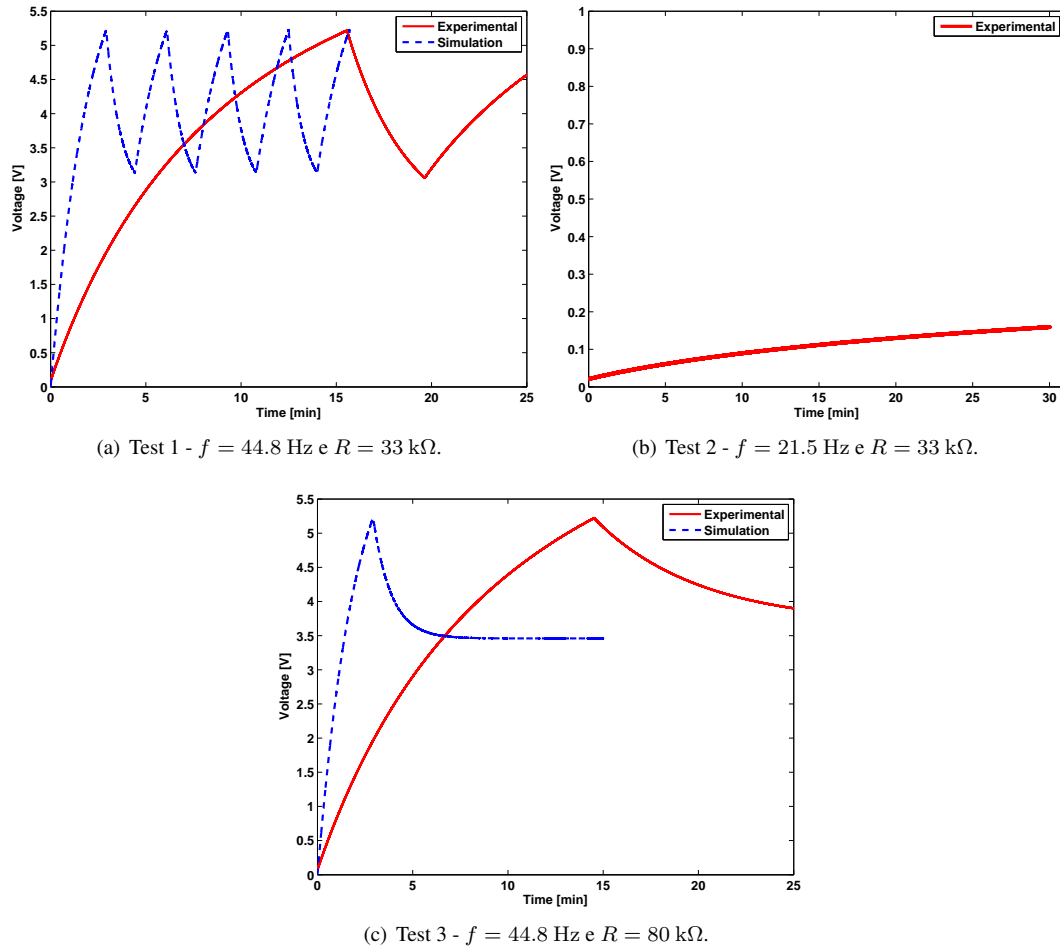


Figure 14. Voltage across the storage capacitor for all performed tests.

The results show that the charging time of the proposed circuit is larger than the charging time of the commercial circuit. This is probably caused by the presence of some micro-controllers and/or operational amplifiers (OP AMP) in the topology of the commercial circuit, which may consume power and cause a voltage drop. Therefore, there is less energy available to charge the capacitor and therefore it takes a longer time to reach the V_H voltage level. Figure 15 presents the result of simulation was carried out with the proposed circuit, considering the same excitation force of test 1, but placing a load before the capacitor to simulate an additional voltage drop of 4.3 V, leading to a larger charging time of almost 10 min, suggesting that this additional load may have caused such difference. Nevertheless, it is worth to note that since the user does not have access to the circuit topology, one can not assure which components cause this voltage drop.

Analyzing Fig. 14, it is also possible to observe that test 2 does not reach V_H because it is not excited at the resonance frequency. An additional test was performed considering $f = 44.80$ Hz and $R_L = 10.00$ k Ω to compare the power delivered to the load, as shows Table 3.

Table 3. Comparison of the results achieved from the experimental tests.

Tests	a_{base} (RMS) [g]	v_{ca} (peak) [V]	t_d [min]	Power (peak) [mW]
1	0.075	8.76	4.07	0.82
2	0.071	0.27	-	-
3	0.075	8.76	> 15	0.34
4	0.075	8.76	0.86	2.72

One may notice that the largest power occurs for the smaller resistance, $R_L = 10$ k Ω , in test 4. This happens because, the EH301A circuit has switching and controlling elements that contributes for the total impedance of the circuit. Hence, the impedance matching situation should also consider the total impedance of the harvesting circuit instead of considering only the impedance of the external load. In addition, the power, calculated by $P = v_L^2/R_L$, is inversely proportional to

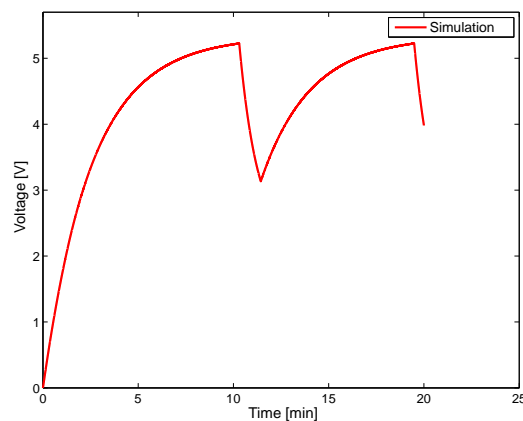


Figure 15. Voltage across the capacitor considering an additional energy consume in the circuit.

the resistive load and, therefore, confirms the larger power for $R_L = 10 \text{ k}\Omega$ among the results presented in Tab. 3. Yet, in case no information is provided, it will be hard to know whether the maximum power extraction condition is satisfied. Regarding the discharge time, it is known that as greater R_L , greater t_d (keeping the capacitance constant). Thus, there is a necessity of finding a balance condition between P and t_d according to the demand and application required.

5. CONCLUSIONS

This paper presented a single degree of freedom model for the piezoelectric harvester obtained by modal parameters estimation. An unified modeling approach was carried out along the simulations regarding both the harvester and extraction/storage circuit, and a comparison between a commercial energy harvesting circuit and three other circuits presented by the authors was performed. Since all circuits presented different topologies and characteristics, their application are also different. The commercial EH301A module could be applied in situations where the external load demands short working period, for instance. On the other hand, the full-wave bridge rectifier could be used in opposite situations, when the external load must be always connected to the circuit. Nevertheless, it is worth noting that the lack of information about the characteristics and operational requirements of the commercial system may lead to some uncertainty about its behavior. For example, if the circuit power output is dependent/independent of the connected external load. Besides, it is very important to carefully choose the components included in the circuits, specially concerning the amount of energy that they may consume. These are very important factors when dealing with energy harvesting and, therefore, must be considered.

6. ACKNOWLEDGEMENTS

The first author is thankful for his scholarship from Coordination for the Improvement of Higher Level Education Personnel (CAPES/Brazil). The authors would like to thank for the financial support provided by National Council for Scientific and Technological Development (CNPq/Brazil) and São Paulo Research Foundation (FAPESP). The authors also would like to thank to CNPq and Minas Gerais State Research Foundation (FAPEMIG) for funding through the National Institute of Science and Technology in Smart Structures (INCT-EIE).

7. REFERENCES

- Advanced Linear Devices, I., 2012. "Eh300/301 epad[®] energy harvesting[™] modules". URL <http://aldinc.com/pdf/EH300ds.pdf>. Acesso em Agosto/2012.
- Anton, S.R. and Sodano, H.A., 2007. "A review of power harvesting using piezoelectric materials (2003-2006)". *Smart Materials and Structures*, Vol. 16, pp. doi: 10.1088/0964-1726/16/3/R01.
- Chen, S.N., Wang, G.J. and Chien, M.C., 2006. "Analytical modeling of piezoelectric vibration-induced micro power generator". *Mechatronics*, Vol. 16, pp. 379-387.
- Chen, Y.Y. and Pan, H.W., 2011. "A piezoelectric vibration energy harvester for tire pressure monitoring systems". In *Proceedings of Symposium on Ultrasonic Electronics*. Vol. 32, pp. 321-322.
- Clementino, M.A., Reginatto, R. and da Silva, S., 2013. "Modeling of piezoelectric energy harvesting considering the dependence of the rectifier circuit". *Journal of the Brazilian Society of Mechanical Sciences & Engineering*, Vol. Aceito para publicação no prelo.
- Cook-Chennault, K.A., Thambi, N., Bitetto, M.A. and Hameyie, E., 2008a. "Piezoelectric energy harvesting: A green and clean alternative for sustained power production". *Bulletin of Science Technology Society*, Vol. 28, pp. 496-509.

M. A. Clementino, C. De Marqui Jr. and S. da Silva
SDOF modeling of a commercial piezoelectric energy harvesting device through experimental identification

- duToit, N.E., Wardle, B.L. and Kim, S.G., 2005. "Design considerations for mems-scale piezoelectric mechanical vibration energy harvesters". *Integrated Ferroelectrics*, Vol. 71, pp. 121–160.
- Elvin, N.G. and Elvin, A.A., 2009. "A coupled finite element-circuit simulation model for analyzing piezoelectric energy generator". *Journal of Intelligent Materials Systems and Structures*, Vol. 20, pp. 587–595.
- Erturk, A. and Inman, D.J., 2008a. "A distributed parameter electromechanical model for cantilevered piezoelectric energy harvesters". *Journal of Vibration and Acoustics*, Vol. 130, p. 041002.
- Erturk, A. and Inman, D.J., 2008b. "Issues in mathematical modeling of piezoelectric energy harvesters". *Smart Materials and Structures*, Vol. 17, p. 065016.
- Erturk, A. and Inman, D.J., 2008c. "On mechanical modeling of cantilevered piezoelectric vibration energy harvesters". *Journal of Intelligent Material Systems and Structures*, Vol. 19, pp. 1311–1325.
- Erturk, A. and Inman, D.J., 2009. "An experimentally validated bimorph cantilever model for piezoelectric energy harvesting from base excitations". *Smart Materials and Structures*, Vol. 18, p. 025009.
- Guyomar, D., Badel, A., Lefeuvre, E. and Richard, C., 2005. "Toward energy harvesting using active materials and conversion improvement by nonlinear processing". *IEEE Transactions on ultrasonics, ferroelectrics, and frequency control*, Vol. 52, pp. 584–595.
- Howells, C.A., 2008. "Piezoelectric energy for soldier systems". Technical report, US Army CERDEC C2D - Army Power Division.
- Inman, D.J., 2001. *Engineering Vibration*. Prentice-Hall Inc., 3rd edition.
- Kalyanaraman, K. and Babu, J., 2010. "Power harvesting system in mobile phones and laptops using piezoelectric charge generation". In *World Congress of Engineering and Computer Science*.
- Kymissis, J., Kendall, C., Paradiso, J. and Gershenfeld, N., 1998. "Parasitic power harvesting in shoes". *Second International Symposium on Wearable Computers*, pp. 132–139. doi:10.1109/ISWC.1998.729539.
- Lallart, M., Garbuio, L., Petit, L., richard, C. and Guyomar, D., 2008. "Double synchronized switch harvesting (dssh): A new energy harvesting scheme for efficient energy extraction". *IEEE Transactions on Ultrasonics, Ferroelectrics and Frequency Control*, Vol. 55, pp. 2119–2130.
- Lallart, M., Richard, C., Garbuio, L., Petit, L. and Guyomar, D., 2011. "High efficiency, wide load bandwidth piezoelectric energy scavenging by a hybrid nonlinear approach". *Sensors and Actuators A*, Vol. 165, pp. 294–302.
- Lefeuvre, E., Audigier, D., Richard, C. and Guyomar, D., 2007. "Buck-boost converter for sensorless power optimization of piezoelectric energy harvester". *IEEE Transactions on Power Electronics*, Vol. 22, pp. 2018–2025.
- Liang, J. and Liao, W.H., 2012. "Improved design and analysis of self-powered synchronized switch interface circuit for piezoelectric energy harvesting systems". *IEEE Transactions on Industrial Electronics*, Vol. 59, pp. 1950–1960.
- Liao, Y. and Sodano, H.A., 2008. "Model of a single mode energy harvester and properties for optimal power generation". *Smart Materials and Structures*, Vol. 17, p. 065026.
- Masana, R. and Daqaq, M.F., 2012. "Energy harvesting in the super-harmonic frequency region of a twin-well oscillator". *Journal of Applied Physics*, Vol. 111, p. 044501.
- Miller, L.M., Halvorsena, E., Dong, T. and Wright, P.K., 2011. "Modeling and experimental verification of low-frequency mems energy harvesting from ambient vibrations". *Journal of Micromechanics and Microengineering*, Vol. 21, p. 045029.
- Pozzi, M., Aung, M.S.H., Zhu, M., Jones, R.K. and Goulermas, J.Y., 2012. "The pizzicato knee-joint energy harvester: characterization with biomechanical data and the effect of backpack load". *Smart Materials and Structures*, Vol. 21, p. 075023.
- Roundy, S. and Wright, P.K., 2004. "A piezoelectric vibration based generator for wireless electronics". *Smart Materials and Structures*, Vol. 13, pp. 1132–1142.
- Sodano, H.A., Inman, D.J. and Park, G., 2004a. "A review of power harvesting using piezoelectric materials". *The Shock and Vibration Digest*, Vol. 36, No. 3, pp. 197–205.
- Sodano, H.A., Inman, D.J. and Park, G., 2004b. "Estimation of electric charge output for piezoelectric energy harvesting". *Strain*, Vol. 40, pp. 49–58.
- Wang, H., Shan, X. and Xie, T., 2012. "Performance optimization for cantilevered piezoelectric energy harvester with a resistive circuit". In *Proceedings of 2012 IEEE International Conference on Mechatronics and Automation*.
- Yang, Y. and Tang, L., 2009. "Equivalent circuit modeling of piezoelectric energy harvesters". *Journal of Intelligent Materials Systems and Structures*, Vol. 20, pp. 2223–2235.

8. RESPONSIBILITY NOTICE

The authors are the only responsible for the printed material included in this paper.